SLAC-PUB-9699
March 2003

Construction of Representative Pore Morphologies in Disordered Nanoporous Two-Phase Materials

Jonathan A. Hedstrom[1], Michael F. Toney[2], Elbert Huang[3], Ho-Cheol Kim[1], Willi Volksen[1], Teddie Magbitang[1], and Robert D. Miller[1]

1 Almaden Research Center, IBM Research Division, 650 Harry Road, San Jose, California, 95120, USA

2 Stanford Synchrotron Radiation Laboratory, Stanford Linear Accelerator Center, 2575 Sand Hill Road, M/S 69, Menlo Park, California 94025, USA

3 TJ Watson Research Center, IBM Research Division, Yorktown Heights, NY 10598, USA

Correspondence to MFT: mftoney@slac.stanford.edu

Abstract

Materials with nanometer size heterogeneities are commonplace in the physical and biological sciences and often exhibit complex morphologies. Although this morphology has a dramatic effect on the materials' properties (e.g., transport and reaction processes), it is often difficult to accurately characterize. We describe a method, using a novel analysis of small angle x-ray scattering data, of generating representative three-dimensional morphologies of isotropic two-phase materials (one class of heterogeneous materials) where the morphology is disordered. This is applied to thin films containing nanometer sized pores with a range of porosities (4-44%). These representations provide a visualization of the pore morphology, give the pore size scale and extent of interconnection, and permit the determination of the transitions from closed pore to interconnected pores to bicontinuous morphology. This methodology will be valuable for characterizing two-phase systems, such as polymer blends, microemulsions, porous geological materials, bones, cements and ceramics.

Submitted to Nature Materials
Work supported in part by the Department of Energy contract DE-AC03-76SF00515.

For heterogeneous materials, a model of the real-space morphology or microstructure is highly desirable, since this allows a better understanding and prediction of the materials properties [1-12]. Two-phase materials with heterogeneities in the nm size scale are often characterized with small angle X-ray and neutron scattering (SAXS and SANS, respectively) [7-12]. These methods provide valuable information, but are not often analyzed to obtain a real space model of the morphology, since this is difficult and may not yield unique results. While some progress has been made in producing real-space morphology or microstructure from SAXS or SANS data on two-phase systems, these analyses are complicated [13,14], involving Monte Carlo methods, or are limited to the isometric case (equal phase volume fractions) [6-9]. Electron microscopies can also be useful for directly determining the morphology of nanoscale heterogeneous materials, but the interpretation of microscopy images is often difficult [15] (due, for example, to limitations in resolution or artifacts created in sample preparation). Here we describe a method for constructing representative real-space morphologies from SAXS [16] data from isotropic two-phase systems with arbitrary phase volume fractions but where the phase morphology is random. This method is applied to nanoporous thin films.

Thin films containing nanometer sized pores are a class of two-phase materials and have potential applications as optical elements [17], low-dielectric-constant interlayer materials for interconnects in semiconductors [15,18], and nanoscopic chemical reactors for catalysis [19] and biotechnology [20]. The pore morphology (i.e., pore size, shape, size distribution, interconnectivity) has a dramatic effect on the nanoporous film properties [21], and hence, is important to understand. These nanoporous films are often formed from two-phase systems that undergo a kinetically arrested phase separation where one component cross links into a

rigid network effectively limiting domain growth and coarsening. Subsequently, the other component (an organic, sacrificial porogen) is expelled from the film through thermolysis at elevated temperatures. Due to the nature of the phase separation mechanism, the isotropic porous microstructures that form have a significantly random component, since there is (random) aggregation of the sacrificial porogen. Thus, the analysis methodology described below is a good approximation. This is certainly the case for films with high porosities where the porous network is formed by a process similar to spinodal decomposition. Our initial work [15] on these films found a broad distribution of pore sizes, which is a manifestation of the random formation process.

The major assumption of our analysis approach is that the three-dimensional, two-phase morphology is sufficiently disordered. Specifically, the morphology can be described by a sum of sinusoidal waves with random orientation and phase, but whose amplitude comes from the SAXS data. While this assumption is not valid for all two-phase systems (e.g., ordered systems), it will likely hold for two-phase materials where the formation process is quasi-random, including early-stage spinodal decomposition [6], sandstones [5], polymer blends and microemulsions [8-10] and other materials with a disordered morphology. Indeed, this assumption is a general strategy for generating two-phase morphologies [1]. As explained above, this assumption is valid for the nanoporous films that we consider. The analysis model uses the SAXS data to generate a function [$\Psi(\mathbf{r})$], which is then clipped to produce the three-dimensional two-phase morphology. Clipping is a process where all points $\mathbf{r}$ with $\Psi(\mathbf{r})$ larger than the clipping parameter α are assigned to one phase, and all other points are considered the other phase. The generated morphology is not a reconstruction of the pore morphology of the material, but is representative of that morphology; it yields X-ray scattering consistent with the experimental SAXS data and hence the lengths between the

morphological features are correctly reproduced. The assumption of randomness is manifest in the generation of $\Psi(\mathbf{r})$ from the empirical data, since this function is the sum of sinusoidal waves with random orientation and phase. To date, this modeling approach has been used to analyze SAXS data [9,10,22] for isometric cases only (both phases have equal volume fractions). We have extended this to non-isometric conditions. This is a significant advance as it allows the comparison of two-phase morphologies under different phase concentrations. More details of the model are given in the methods section.

We have used this new method of analysis on a series of nanoporous thin films that were generated with porogen loadings from 5% to 50% (weight percent porogen). The porosity of the films was determined by X-ray reflectivity [23,24] and range from 4% to 44% (5 and 50% loading, respectively). The porosity determines the clipping parameter. The pore morphologies were generated in cubic volumes with side lengths of 50 nm – 600 nm. Figure 1 shows representative morphologies as a function of porogen loading for a 200 nm cube. Yellow corresponds to the methyl silsesquioxane (MSSQ) matrix and the red depicts the pore interior as seen through the cube side. These visualizations provide a better understanding of the pore network and allow a more detailed characterization of the morphology. First, Fig. 1 shows that as the loading increases, the average pore size increases. This is consistent with the previous analysis [15], which modeled the SAXS data as hollow, non-overlapping spheres with a distribution of diameters. Indeed, quantitative comparison of pore sizes deduced from Fig. 1 agrees well with the sphere model for the 5 -15% loadings. Specifically, the average pore radii extracted from the data in figure 2 are 2.0, 2.1 and 2.4 nm for the 5%, 10% and 15% loadings respectively. This compares well with 1.5, 1.7, and 2.2 nm as determined with the previous analysis [15]. Above 15%, the morphology becomes bicontinuous [25] (vide infra) and one cannot easily define an average pore size. Indeed, also evident in Fig. 1 is that

at about 15% loading, the pores have become significantly interconnected (although it is not clear from this figure if the morphology is bicontinuous).

It is important to determine the porogen loading where the pore morphology becomes bicontinuous, since in this case, the films may not be impervious to ingress of processing liquids, lining barrier materials, and plated metals. The determination of the transition to a bicontinuous morphology is of generic interest in two-phase materials, since this transition has a large impact on the transport and reaction properties in these materials. In analyzing these morphologies, several methods have been applied to determine the transition to a bicontinuous morphology. Inspection of Fig. 1 suggests that this occurs near 30% loading, but this is not accurate as this visualization predominantly shows the cube surface and not the interior. Figure 2 uses a better procedure for visualizing and identifying this transition. Here, the MSSQ matrix is transparent and the pores are shown as seen from outside the cube. The largest pore is colored red (left side) and this pore is removed on the right side of the figure. In systems with higher porogen loadings, the elimination of the largest pore results in the removal of most of the pore volume. Thus, it is evident from Fig. 2 that the 25 and 40% loadings are bicontinuous, while the 15% appears to be just highly interconnected (not quite bicontinuous).

Figure 3 shows a more quantitative method of determining the transition to a bicontinuous structure. This plots the number of pores contained in the cube as a function of the cube side. For completely isolated pores, the number of pores should scale with the cube volume (solid lines). For a bicontinuous structure, ideally there is only one large pore; however, portions of this pore located at the cell boundary may be perceived as isolated pores, since the pore region connected these to the bicontinuous porous structure may lie outside the viewed

region. Consequently, the number of pores for a bicontinuous structure will approximately scale with the surface area (dashed lines). Figure 3 shows that the transition to a bicontinuous morphology occurs between 15 and 25% loadings. This is in good agreement with data obtained by positron annihilation spectroscopy [26=apl2002,27] for similar systems. The determination of this transition to a bicontinuous microstructure is only possible since we can model non-isometric compositions and is an important result of this work.

We have further tested the validity of this modeling approach. First, we have calculated the surface-to-volume (S/V) ratio from the raw SAXS data [11,28] and from the model-dependent spectral function [29] and have compared these to typical morphologies obtained from the modeling. For all porogen loadings, we have found excellent quantitative agreement for S/V for all three methods. Second, we have applied this analysis to another system [29.5] and find that the pore morphology is significantly different from that shown in Fig. 1 and that the transition to a bicontinuous morphology occurs at a different porogen loading. These tests provide support for the applicability of this analysis methodology.

The methodology we have described will be valuable for characterizing a wide variety of two-phase systems that are formed by a random process. This will include polymer blends [9], microemulsions [10], porous geological materials [30], bones [31], cements [12] and ceramics [32]. Since the method is applicable for a range of phase volume fractions, it will be possible to determine the transitions between different types of morphologies (e.g., closed-cell to bicontinuous), which will permit better understanding of properties such as transport in two-phase materials. While the approach we have described has been limited to two-phase systems, the morphologies of more complicated heterogeneous materials (e.g., three-phase systems) can be determined using a similar approach. This will, however, require several

small-angle scattering data sets that isolate the scattering from each two of the three phases [33].

Methods

Sample Preparation

To produce these nanoporous films, methyl silsesquioxane (MSSQ) (M_w=15k, Dow Corning) and the sacrificial organic porogen are dissolved in a mutual solvent (e.g., propylene glycol methyl ether), spin coated onto Si substrates, and annealed under a N_2 atmosphere at 450 °C for one hour after an initial ramp rate of 5 °C/min [15,23,34]. The porogen is a copolymer poly(methyl methacrylate-*co*-dimethylaminoethyl methacrylate), or P(MMA-*co*-DMAEMA), which was synthesized by atom transfer radical polymerization [M_w=12k, PDI=1.1]. Typical film thicknesses were about 1 μm.

The SAXS experiments were performed at the IMM-CAT at the Advanced Photon Source at Argonne National Laboratory. The incident X-rays from an undulator were monochromatized with a Ge (111) crystal to an energy of 7.66 keV. Slits confined the incidence beam size to either 100 x 100 μm (high resolution) or 200 x 200 μm (low resolution). An area detector was used with a sample-to-detector distance of either 2750 mm (high resolution) or 235 mm (low resolution). The high and low resolution data sets were merged and the SAXS from the MSSQ was subtracted from the merged data to give the SAXS from the pores.

Analysis Methodology

The method we describe builds on work by Cahn [6] aimed at producing three-dimensional structures formed by spinodal decomposition and extended by Berk [7,7.5] to analyze scattering data from bicontinuous structures. Here a Gaussian random function [$\Psi(\mathbf{r})$] is generated by the superposition of many sinusoidal waves with random directions and phases.

This function is then clipped to produce a representative three-dimensional morphology: all points **r** with $\Psi(\mathbf{r}) > \alpha$ are assigned to one phase, and all other points are in the other phase. The clipping parameter α is determined by the porosity. The wavevectors for the sinusoidal waves are obtained from a spectra function [f(k)], which gives the characteristic wavelengths of the physical morphology and thus describes the essential morphological features. Often [6-8] there is an assumed form for the spectral function. Rather than using this assumed form (which failed to describe our data), we have directly obtained the spectral function from the scattering data using the method from Ref. [9]. This insures that the generated morphology yields X-ray scattering consistent with the experimental data and that the length scales of the morphological features ion the two-phase material are faithfully reproduced. One significant limitation to the methods of Refs. [6,8,9] is that they are limited to isometric cases (both phases have equal volume fractions). Since the random function $\Psi(\mathbf{r})$ is defined to have a mean value of 0, the isometric clipping parameter is α=0, which insures equal volume fractions. We have extended this approach to non-isometric volume fractions using results from Ref. [29]. The clipping parameter, α, can be non-zero with a resulting unequal volume fraction. This is a significant advance as it allows the comparison two-phase morphologies for varying phase-volume fractions.

The analysis procedure is illustrated in Fig. 4. First, the SAXS data I(q) are Fourier transformed to produce the Debye correlation function Γ^{α}(r),

$$\Gamma^{\alpha}(r) = \int_0^{\infty} 4\pi q^2 I(q)[\sin(qr)/(qr)]dq. \quad (1)$$

Here $q=(4\pi/\lambda)\sin(\theta/2)$, where λ and θ are the X-ray wavelength and the scattering angle, respectively. This is normalized such that $\Gamma^{\alpha}(\infty)=(\Gamma^{\alpha}(0))^2$ and is related to the correlation function, g(r), of $\Psi(\mathbf{r})$ by [29]

$$\Gamma^{\alpha}(r) = \Gamma^{\alpha}(0) - (\frac{1}{2\pi}) \int_{g(r)}^{1} \frac{\exp[-\alpha^2/(1+t)]}{\sqrt{1-t^2}} dt, \quad (2)$$

where $\Gamma^{\alpha}(0)$ is the volume fraction of one of the phases (e.g., porosity) and is related to the clipping parameter α by

$$\Gamma^{\alpha}(0) = \frac{1}{\sqrt{2\pi}} \int_{\alpha}^{\infty} \exp[-x^2/2] dx. \quad (3)$$

The spectral function of the Gaussian random function $\Psi(\mathbf{r})$ is then obtained by the inverse Fourier transform

$$f(k) = \int_{0}^{\infty} 4\pi r^2 g(r) [\sin(kr)/(kr)] dr. \quad (4)$$

The function $\Psi(\mathbf{r})$ is generated by summing many (N=10000) sinusoidal waves

$$\Psi(r) = \sqrt{2N} \sum_{i=1}^{N} \cos(\mathbf{k}_i \cdot \mathbf{r} + \phi_i), \quad (5)$$

where the directions of wavevectors $\mathbf{k}_i$ and phases φ_i are random, but the magnitudes of wavevectors $\mathbf{k}_i$ are obtained from the spectral function given by Eq. (4). To obtain the morphologies, the field is then clipped to the corresponding α calculated in Eq. (3). All points $\mathbf{r}$ with $\Psi(\mathbf{r})>\alpha$ are assigned to one phase and all other points are assigned to the other phase.

References

[1] Levitz, P. Off-lattice reconstruction of porous media: critical evaluation, geometrical confinement and molecular transport. *Adv. Coll. Inter. Sci.* **76-77** 71-106 (1998).

[2] *Porous Media: Geometry and Transports*, Adler, P.M. (Butterworth-Heinemann, Boston, 1992).

[3] Golden, K.M. Brine percolation and the transport of sea ice. *Ann.Glacio.* 33, 28-36 (2001).

[4] Spanne, P., Thovert, J.F., Jacquin, C.J., Lindquist, W.B., Jones, K.W. & Alder P.M. Synchrotron Computed Microtomography of Porous media: topology and transports. *Phys. Rev. Lett.* **73**, 2001-2004 (1994).

[5] Manwart, C., Torquato, S. & Hilfer R. Stochastic reconstruction of sandstones. *Phys. Rev. E* **62**, 893-899 (2000).

[6] Cahn, J.W. Phase Separation by Spinodal decomposition in isotropic systems. *J. Chem. Phys.* **42**, 93 (1965).

[7] Berk, N.F. Scattering Properties of a Model Bicontinuous Structure with a Well Defined Length Scale. *Phys. Rev. Lett.* **58**, 2718 (1987); Berk, N.F. Scattering Properties of a the leveled-wave model of random morphologies. *Phys. Rev. A* **44**, 5069 (1991).

[8] Chen, S.-H., Lee, D.D., Kimishima, K., Jinnai, H. & Hashimoto, T. Measurement of the Gaussian curvature of the surfactant film in an isometric bicontinuous one-phase microemulsion. *Phys. Rev. E* **54**, 6526-6531 (1996).

[9] Jinnai, H., Nishikawa, Y., Chen, S.-H., Koizumi, S., & Hashimoto, T. Morphological Characterization of bicontinuous structures in polymer blends and microemulsions by the inverse-clipping method in context of the clipping-random-wave model. *Phys. Rev. E* **61**, 6773 (2000).

[10] Choy, D., & Chen, S.-H. Clipped random wave analysis of isometric lamellar

microemulsions. *Phys. Rev. E* **61**, 4148-4155 (2000).

[11] Guinier, A. & Fournet, C. *Small-angle X-ray Scattering*, (Wiley, New York, 1955).

[12] Haussler, F., Hempel, M., Baumbach, H. & Tritthart, J. Off-lattice reconstruction of porous media: critical evaluation, geometrical confinement and molecular transport. *Adv. Cement Res.* **13** 65-73 (2001).

[13] Rozman, M.G. & Utz, M. Efficient reconstruction of morphologies from correlation functions. *Phys. Rev. E* **63**, 6701-6709 (2001).

[14] Manwart, C. & Hilfer R.M. Reconstruction of random media using Monte Carol methods. *Phys. Rev. E* **59**, 5596-5599 (1999).

[15] Huang, E., Toney, M.F., Volksen, W., Mecerreyes, D., Brock, P., Kim, H.-C., Hawker, C.J., Hedrick, J.L., Lee, V.Y., Magbitang, T., Miller R.D. & Lurio, L.B. Pore Size Distributions in Nanoporous Methylsilsesquioxanes (MSSQ) Films as Determined by Small Angle X-Ray Scattering (SAXS). *Appl. Phys. Lett.* **81**, 2232-2234 (2002).

[16] While we will be specific to SAXS in the remaining discussion, the method is equally applicable to SANS.

[17] Walheim, S., Schaffer, E., Mlynek, J. & Steiner, U. Nanophase-seperated polymer films as high-performance antireflection coatings. *Science* **283**, 520-522 (1999).

[18] *Low Dielectric Constant Materials for IC Applications*, P.S. Ho, J. Leu, W.W. Lee, eds., (Springer-Verlag, Berlin, 2002).

[19] Stein, A., Melde, B.J., & Schroden, R.C. Hybrid Inorganic-Organic mesoporous silicates-nanoscopic reactors coming of age. *Adv. Mater.* **12**, 1403-1419 (2000).

[20] Lei, C., Shin, Y., Liu, J., & Ackerman, E.J. Entrapping in a functionalized nanoporous support. *J. Am. Chem. Soc.* **124**, 11242-11243 (2002).

[21] Petkov, M.P., Weber, M.H., Lynn, K.G., Rodbell, K.P. & Cohen, S.A. Open volume defects (measured by positron annihilation spectroscopy) in thin film hydrogen-

silsesquioxane spin-on-glass; correlation with dielectric constant. *J.. Appl. Phys.* **86**, 3104-3109 (1999).

[22] Chen, S.-H & Chang, S.-L. Simulation of bicontinuous microemulsions : comparison of simulated real-space microstructures with scattering experiments. *J. Appl. Cryst.* **24**, 721-731 (1991).

[23] Nguyen, C.V., Carter, K.R., Hawker, C.J., Hedrick, J.L., Jaffe, R.L., Miller, R.D., Remenar, J.F., Rhee, H.-W., Rice, P.M., Toney, M.F., Trollsaes, M., & Yoon, D.Y. Low-Dielectric Constant, Nanoporous Organosilicate Films Prepared via Organic/Inorganic Polymer Hybrid Templates. *Chem. of Materials* **111**, 3080-3085 (1999).

[24] Bolze, J., Ree, M., Youn, H.S., Chu, S.-H., & Char, K. Synchrotron X-ray Reflectivity Study on the Structure of Templated Polyoganosilicate Thin Films and Their Derived Nanoporous Analogues. *Langmuir* **17**, 6683-6691 (2001).

[25] In a bicontinuous structure, it is possible to completely traverse the material which completely remaining in either of both phases.

[26] Wang, C.L., Weber, M.H., Lynn, K.G. & Rodbell, K.P. Nanometer-scale pores in low-k dielectric films probed by positron annihilation lifetime spectroscopy. *Appl. Phys. Lett.* **81**, 4413-4415 (2002).

[27] Petkov, M.P., Weber, M.H., Lynn, K.G. & Rodbell, K.P. Probing capped and uncapped mesoporous low-dielectric constant films using positron annihilation lifetime spectroscopy. *Appl. Phys. Lett.* **77**, 2470-2772 (2000).

[28] Glatter, O. *Small-angle X-ray Scattering*, (New York).

[29] Teubner, M. Level Surfaces of Gaussian Random Fields and Microemulsions. *Europhys. Lett.* **14**, 403 (1991).

[29.5] Rajagopalan, T., Sun, J., Lahlouh, B., Lubguban, J.A., Huang, D.H., Biswas, N., Simon, S.L., Gangopadhyay, S., Mallikarjunan, Kim, H.-C., Volksen, W., Toney, M.F.,

Huang, E., Rice, P.M., Delenia, E. & Miller, R.D. Supercritical Carbon Dioxide Extraction of Porogens for the preparation of ultralow dielectric constant films. Submitted to *Appl. Phys. Lett.*, 2002.

[30] Sen, D., Mazumder, S., & Tarafdar, S. Pore morphology and pore surface roughening in rocks: a small angle neutron scattering investigation. *J. Mater. Sci.* **37**, 941-947 (2002).

[31] Corwin, S. C. Bone poroelasticity. *J. Am. Biomech.* **32**, 217-238 (1999).

[32] Schaefer, D.W., Brow, R.K., Olivier, B.J., Rieker, T., Beaucage, G., Hrubesh, L. & Lin, J.S. in *Modern Aspects of Small Angle Scattering*, Brumberger, H., ed., (Kluwer, Amesterdam, 1995), 299-397.

[33] Bumajdad, A., Eastoe, J., Griffiths, P., Steytler, D.C., Heenan, R.K., Lu, J.R., & Timmins, P. Interfacial compositions and phase structures in mixed microemulsions. *Langmuir* **15**, 5271-5278 (1999).

[34] Hedrick, J.L., Miller R.D. Hawker, C.J., Carter, K.R., Volksen, W., Yoon, D. & Trollsas, M. Templating nanoporousity in Thin Film dielectric insulators. *Adv. Mater.* **10**, 1049-1053 (1998).

Acknowledgements:

The SAXS experiments were performed on the IMMY-CAT beamline at the Advanced Photon Source at Argonne national Laboratory, which is supported by the U. S. Department of Energy, Office of Science, Office of Basic Energy Sciences, under Contract No. W-31-109-ENG-38. Some program funding was provided by the NIST-ATP cooperative agreement No. 70NANB8H4013.

Figures

1. Visualizations of representative microstructures as function of porogen loading for 200 nm cubes. Yellow represents the MSSQ matrix and the pore interior is highlighted in red as seen through the cube sides.
2. Images of microstructures for 10-40% loadings for a cube side of 200 nm. The MSSQ matrix is transparent and the pores are shown as seen from outside the cube. Left side shows all the pores with the largest pore colored in red. This largest pore is removed on the right side.
3. The number of pores contained in the cube as a function of the cube side. Solid lines vary as the cube of the side length, while dashed lines vary as the square of the side length.
4. Schematic illustration of the analysis process. The experimental data, I(q), are shown by the solid line, while the spectral function f(k) is given by the dashed line. I(q) has been extrapolated to high q as q^{-4}. The inset shows a histogram of $\Psi(\mathbf{r})$ and a typical α.

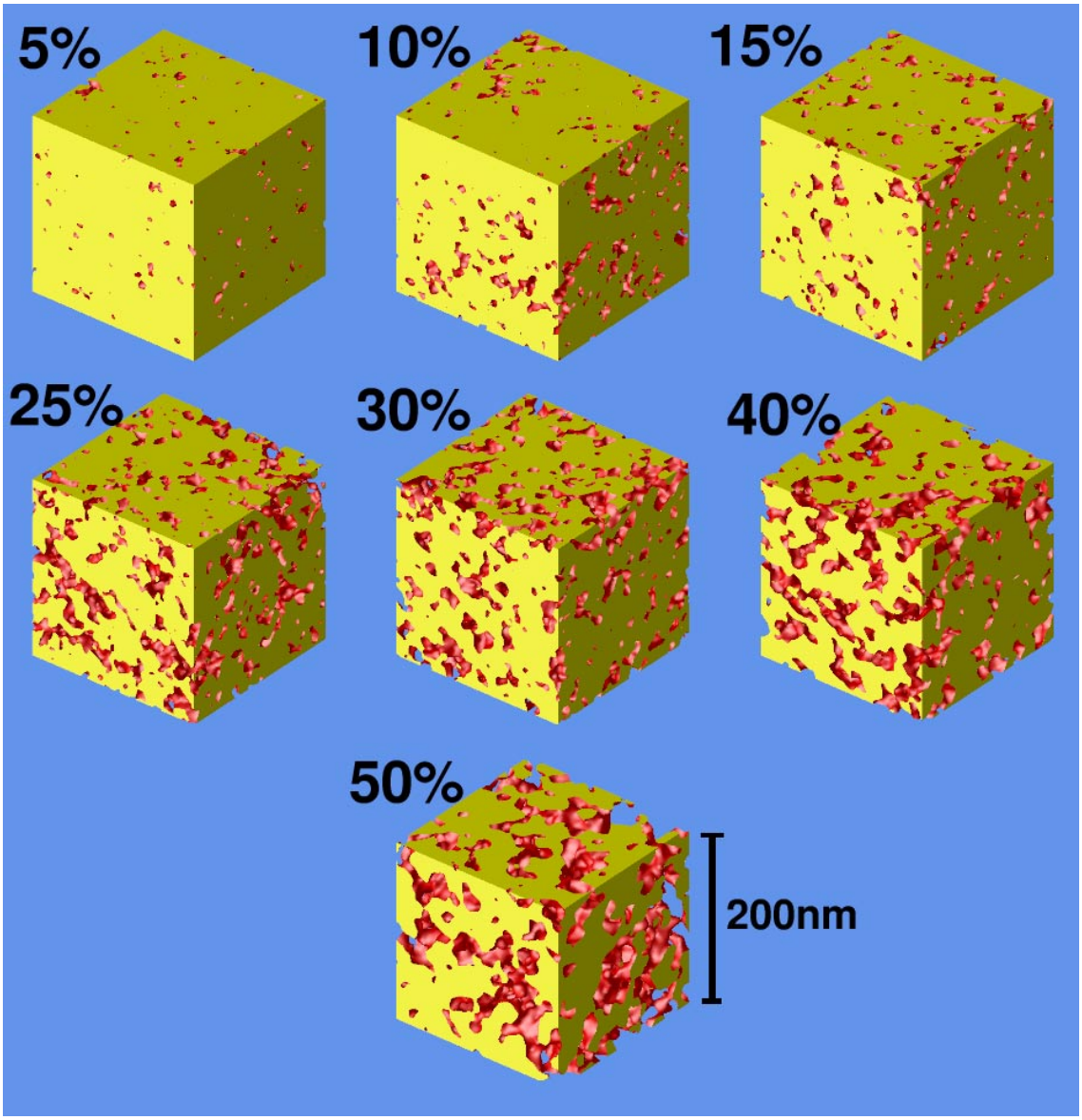

Fig 1

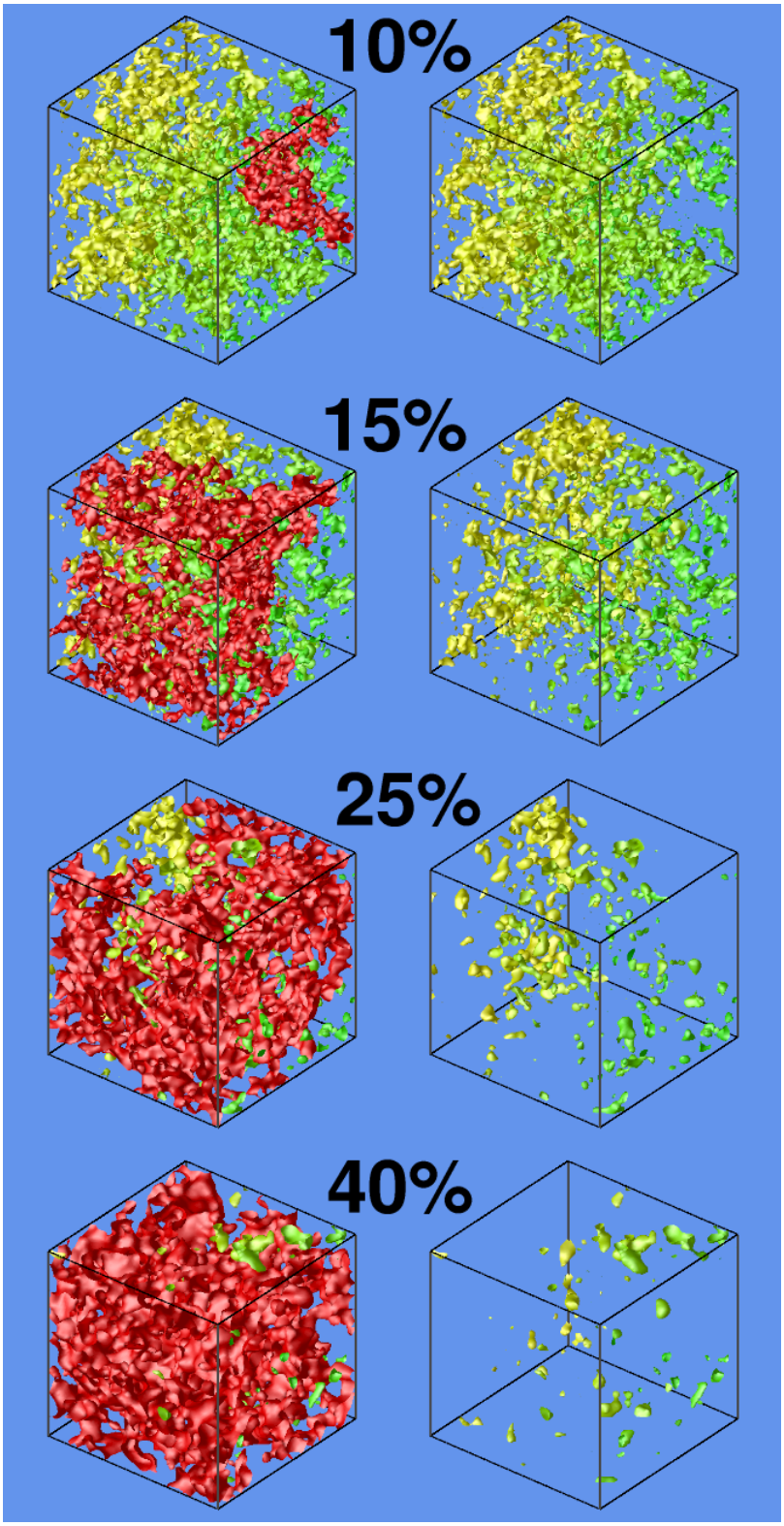

Fig 2

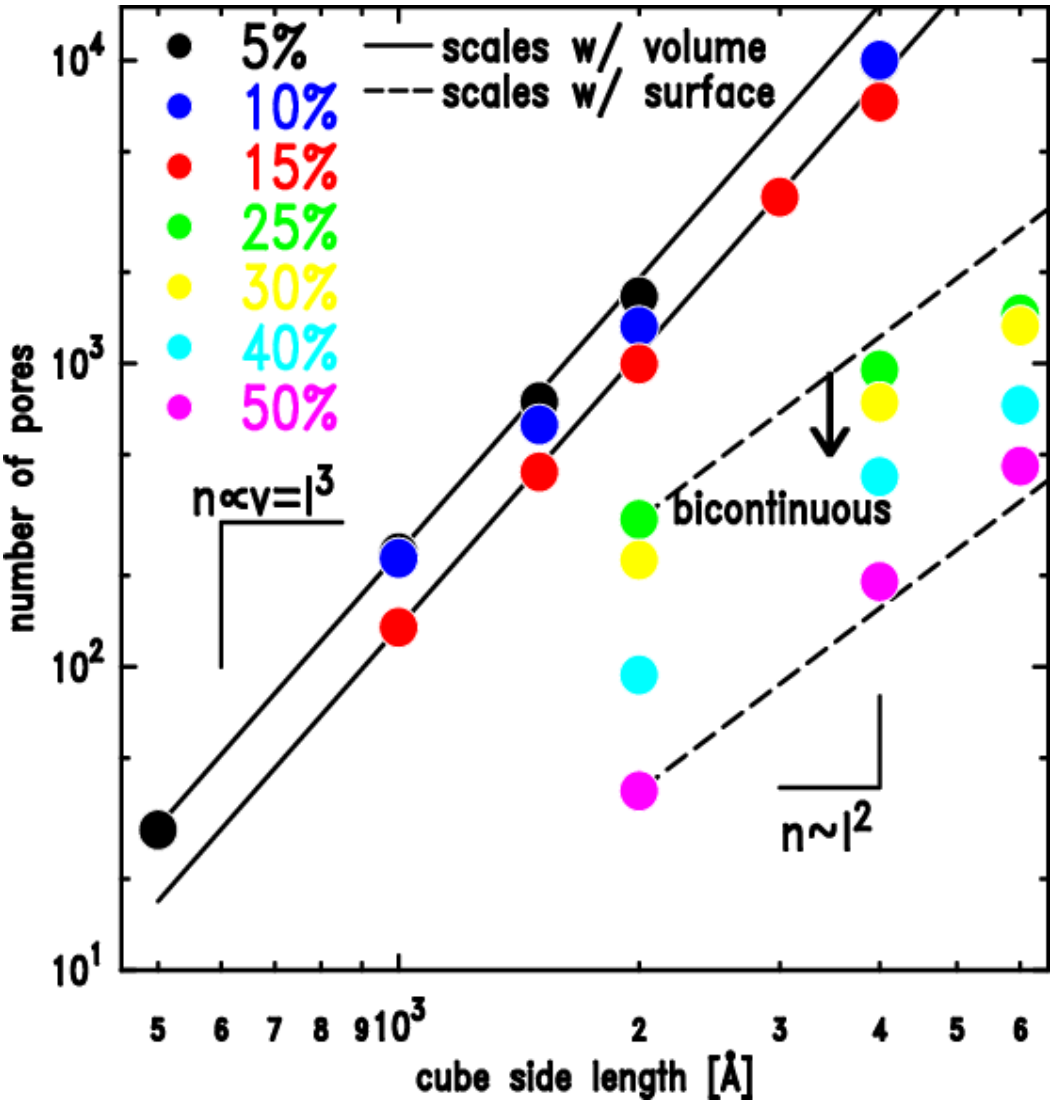
5%
10%
15%
25%
30%
40%
50%
scales w/ volume
scales w/ surface
n∝v=l^3
bicontinuous
n~l^2
number of pores
cube side length [Å]
10^4
10^3
10^2
10^1
5 6 7 8 9 10^3 2 3 4 5 6

Fig 3

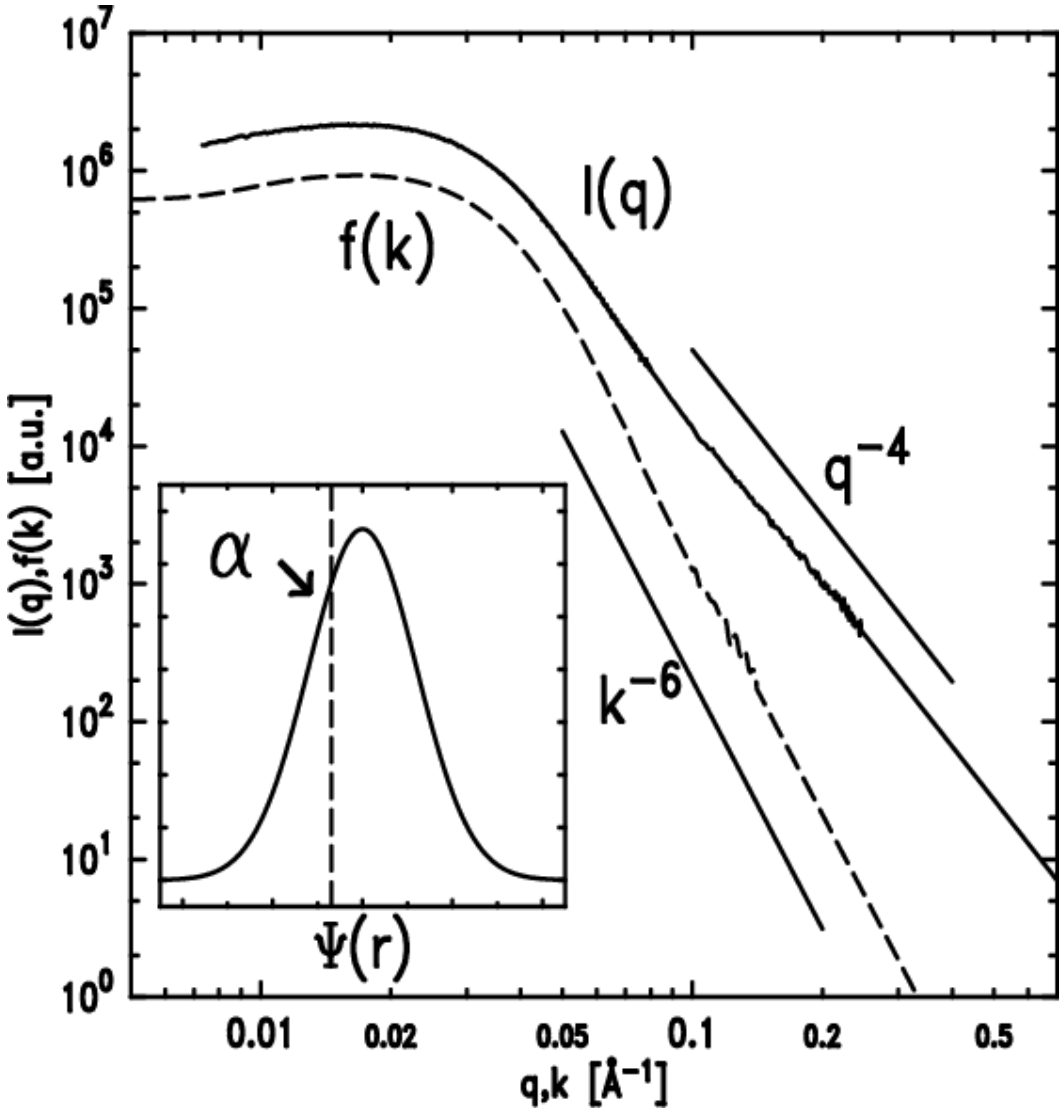
I(q)
f(k)
q^-4
k^-6
α
Ψ(r)
I(q),f(k) [a.u.]
q,k [Å^-1]
10^7
10^6
10^5
10^4
10^3
10^2
10^1
10^0
0.01
0.02
0.05
0.1
0.2
0.5

Fig 4